

Lattice dynamics in the spin-1/2 frustrated kagome compound herbertsmithite

Ying Li*,^{1,2} A. Pustogow*,³ M. Bories,³ P. Pupal,⁴ C. Krellner,⁴ M. Dressel,³ and Roser Valentí²

¹*Department of Applied Physics and MOE Key Laboratory for Nonequilibrium Synthesis and Modulation of Condensed Matter, School of Science, Xi'an Jiaotong University, Xi'an 710049, China*

²*Institut für Theoretische Physik, Goethe-Universität Frankfurt, Max-von-Laue-Strasse 1, 60438 Frankfurt am Main, Germany*

³*1. Physikalisches Institut, Universität Stuttgart, Pfaffenwaldring 57, D-70569 Stuttgart Germany*

⁴*Physikalisches Institut, Goethe-Universität Frankfurt, 60438 Frankfurt am Main, Germany*

(Dated: February 12, 2020)

We investigate the lattice dynamics in the spin-1/2 frustrated kagome compound herbertsmithite $\text{ZnCu}_3(\text{OH})_6\text{Cl}_2$ by a combination of infrared spectroscopy measurements and *ab initio* density functional theory calculations, and provide an unambiguous assignment of infrared-active lattice vibrations involving in-plane and out-of-plane atom displacements in the kagome layers. Upon cooling, non-thermal red-shifts and broadening appear specifically for modes that deform the kagome layer or affect the Cu-O-Cu bond angles, thus creating pronounced modifications of the antiferromagnetic exchange coupling. Our results indicate the presence of a strong magnetoelastic coupling to the spin system. We discuss the effects of this coupling and its relation to recent experiments reporting a global symmetry reduction of the kagome lattice symmetry.

The nature of the ground state in the frustrated spin-1/2 kagome compound $\text{ZnCu}_3(\text{OH})_6\text{Cl}_2$ has been subject of intense discussion for many years^{1,2}. Being a perfect realization of a kagome lattice of spin-1/2 Cu atoms with dominant nearest-neighbor Heisenberg antiferromagnetic interactions, $J \approx 180$ K,³ this material was suggested to be a canonical candidate for bearing a quantum-spin-liquid (QSL) state. Indeed, the Cu^{2+} magnetic moments do not order⁴ down to the lowest measured temperatures and excitations are dominated by a rather unconventional broad continuum⁵. While these features strongly indicate a QSL ground state, there is presently a lot of debate, both from the experimental and theoretical side, concerning its nature^{4,6–17}. Interestingly, recent studies on herbertsmithite have invoked different aspects of this compound, such as interlayer Cu/Zn antisite disorder¹⁸ and lattice effects¹⁹ to investigate this question. Actually, such effects uncover a rich behavior in these systems. For instance the authors of Ref. 19 identify via non-linear optical response experiments a subtle high-temperature monoclinic distortion in herbertsmithite that is suggested to influence the nature of the QSL ground state. Such symmetry reduction was also reported in previous torque and electron-spin-resonance (ESR) studies²⁰. Its origin and relation to the underlying spin system, however, remain unsettled. The knowledge on the nature of the vibrational modes in this system and the magnetoelastic coupling would be of major help to resolve these questions. In fact, there has already been considerable spectroscopic work on herbertsmithite investigating phononic, electronic and magnetic excitations^{21–23}. Specifically, recent infrared spectroscopy studies on the title compound and other frustrated systems revealed anomalous broadening and red shifts of vibrational modes upon cooling,^{21,24,25} as opposed to the narrowing and hardening arising from the usual thermal effects. It was suggested that these anomalies are related to the coupling to the spin system.

In view of these findings, we performed an extensive theoretical and spectroscopic study of the vibrational features in $\text{ZnCu}_3(\text{OH})_6\text{Cl}_2$. Via *ab initio* phonon calculations we provide a one-to-one assignment of phonon modes and the involved lattice sites. We observe non-thermal broadening and red-shift for low-frequency vibrations in the range of expected strong spin fluctuations. Notably, we identify these low-frequency vibrations to be related to atomic motions that deform the kagome layers and modify the Cu-O-Cu bond angles directly affecting the antiferromagnetic Cu-Cu exchange interactions and therefore influencing the underlying magnetism.

Single crystals of $\text{ZnCu}_3(\text{OH})_6\text{Cl}_2$ were prepared by hydrothermal synthesis²⁶. The optical reflectivity was measured on as-grown surfaces of mm-sized samples covering frequency and temperature ranges of 40–20 000 cm^{-1} and 10–295 K, respectively, and combined with the VIS-UV data reported elsewhere²². Standard extrapolations towards low and high frequencies were applied in order to determine the optical conductivity using the Kramers-Kronig relations.

Ab initio vibrational studies were performed using the crystal structure of $\text{ZnCu}_3(\text{OH})_6\text{Cl}_2$ given in the space group $R\bar{3}m$ ²⁷. The phonon frequencies and eigenvectors were calculated by diagonalizing the dynamical matrices using the phonopy package^{28,29}. The dynamical matrices were constructed from the force constants determined from the finite displacements in $2 \times 2 \times 1$ supercells³⁰ performing density functional calculations within the Perdew-Burke-Ernzerhof parametrization of the generalized gradient approximation³¹ and using the projector augmented wave approximation³² implemented in the Vienna package (VASP)^{33–35}. The Brillouin zone for the supercell was sampled with a $4 \times 4 \times 4$ \mathbf{k} point mesh, and the plane-wave cut-off was set at 520 eV.

In Fig. 1(c,d) we show the polarized infrared reflectivity spectra of $\text{ZnCu}_3(\text{OH})_6\text{Cl}_2$ and compare them to the calculated phonon mode frequencies shown in Fig. 1(a-b).

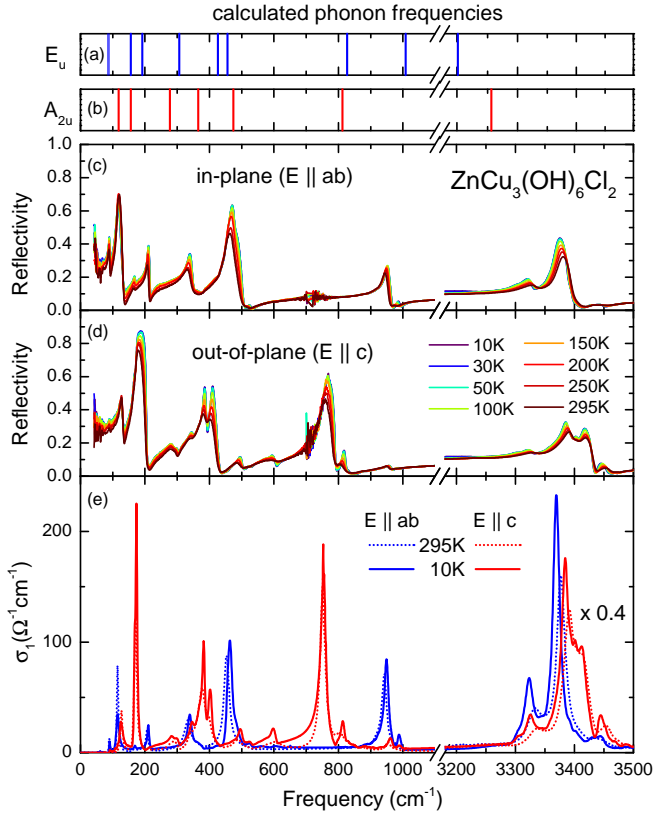


FIG. 1. (a,b) Phonon calculations yield good agreement with polarized infrared spectra of $\text{ZnCu}_3(\text{OH})_6\text{Cl}_2$. Note the E_u doublet at 84.8 and 88.4 cm^{-1} ; all E_u and A_{2u} mode frequencies are listed in Table I. (c,d) The temperature-dependent in- and out-of-plane reflectivity is dominated by vibrational features in the entire infrared range. (e) The corresponding optical conductivity was calculated using the Kramers-Kronig relations. For convenience, only 295 K (dotted) and 10 K (solid lines) spectra are shown for both orientations.

The optical absorption in herbertsmithite arises mainly from phonons since the strong Coulomb repulsion in this system yields a charge gap of more than 3 eV²². This is in contrast to the case of triangular-lattice organic QSL candidates, where electronic transitions between the Hubbard bands are the dominant contribution in the far- and mid-infrared range^{36–38}. While vibrational calculations have been carried out and discussed also on the molecular solids^{39,40}, the absence of an electronic back-

TABLE I. The infrared-active doubly-degenerate E_u modes and infrared-active out-of-plane A_{2u} modes in cm^{-1} for $\text{ZnCu}_3(\text{OH})_6\text{Cl}_2$ obtained by *ab initio* calculations.

E_u^1	E_u^2	E_u^3	E_u^4	E_u^5	E_u^6	E_u^7	E_u^8	E_u^9
84.8	88.4	155.8	191.8	306.5	426.1	455.8	826.5	1008.7
A_{2u}^1	A_{2u}^2	A_{2u}^3	A_{2u}^4	A_{2u}^5	A_{2u}^6	A_{2u}^7	E_u^{10}	
117.9	155.9	277.2	365.1	473.8	812.4	3256.3	3201.5	

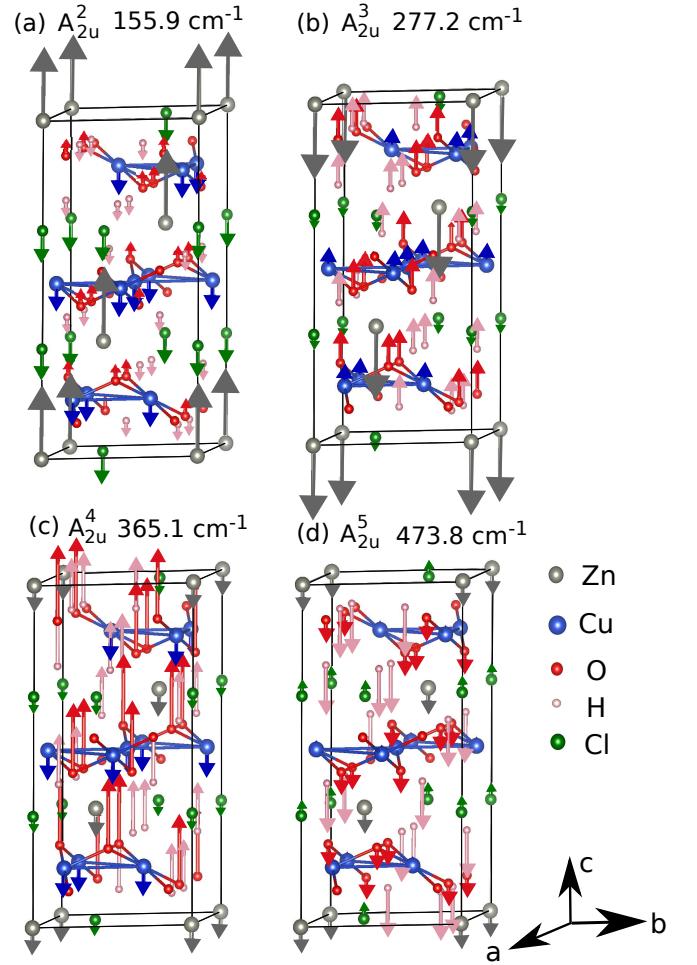


FIG. 2. The A_{2u} modes at (a) 155.9 cm^{-1} (b) 277.2 cm^{-1} (c) 365.1 cm^{-1} and (d) 473.8 cm^{-1} according to our *ab initio* calculations. The atomic motions of these infrared vibrations were projected along the crystallographic c -axis.

ground in $\text{ZnCu}_3(\text{OH})_6\text{Cl}_2$ allows for an undisturbed investigation of the coupling between magnetic excitations and the lattice. In Fig. 1(c,d) the anisotropy and temperature dependence of the in-plane (electric field $E \parallel ab$) and out-of-plane reflectivity ($E \parallel c$) agree well with previous reports^{21,41}, confirming our excellent sample quality. We plot the corresponding optical conductivity at room temperature and at 10 K in Fig. 1(e).

Herbertsmithite in the $R\bar{3}m$ structure has 18 atoms in the primitive unit cell and $18 \times 3 = 54$ phonon modes are expected. Our calculations display all 54 phonon modes as previously classified²¹ including 10 infrared-active doubly-degenerate E_u in-plane modes ($E \parallel ab$, Fig. 1(a)) and 7 infrared-active out-of-plane modes A_{2u} ($E \parallel c$ Fig. 1(b)). The frequencies are shown in Table I. Full phonon modes can be found in the Supplemental Material⁴². Our calculations agree well with our measured optical spectra (Fig. 1(c-e)). Especially at low frequencies we can unambiguously assign the experimentally observed peaks to the computational results. The atomic

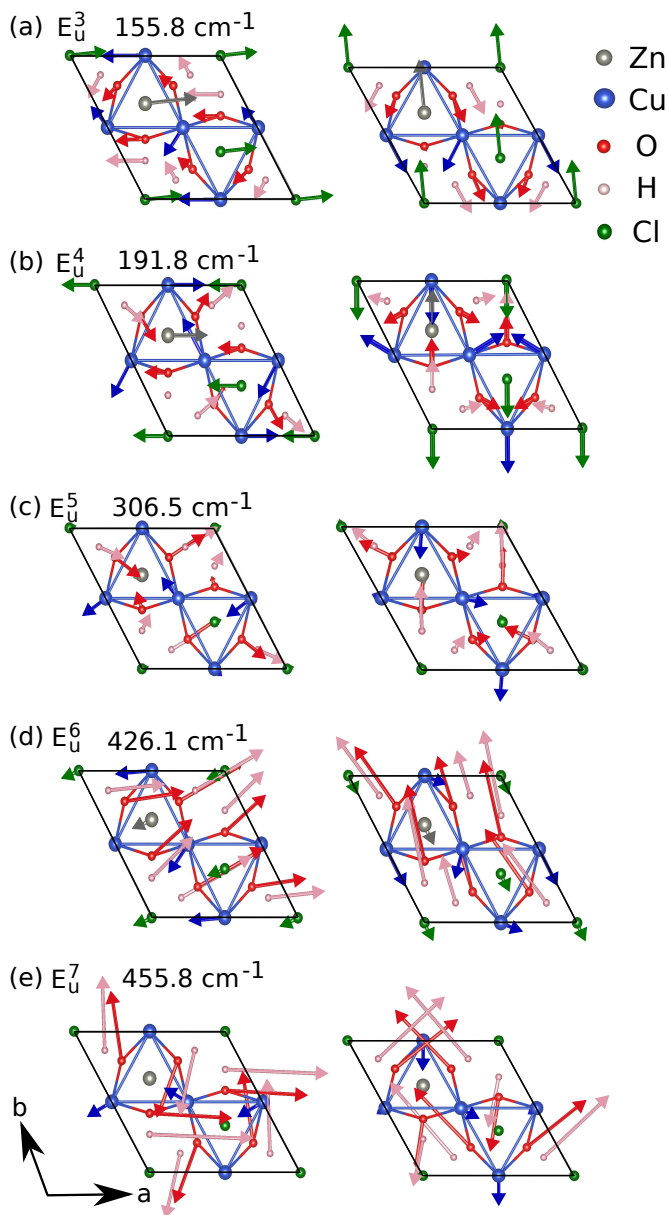


FIG. 3. The doubly-degenerate E_u infrared vibration modes at (a) 155.8, (b) 191.8, (c) 306.5, (d) 426.1, and (e) 455.8 cm^{-1} according to our *ab initio* calculations. The arrow sizes and lengths correspond to the relative amplitudes of the modes, which are projected on the ab -plane.

motions of the infrared vibrations between 150 and 500 cm^{-1} are displayed in Fig. 2 for the A_{2u} modes (projected along c direction) and Fig. 3 for the E_u modes (projected onto the ab plane). The total dipole moment of the A_{2u} modes parallel to the ab plane and for the E_u modes along c direction is zero, consistent with the polarized infrared spectra. While the lattice vibrations are dominated by Zn, Cl and Cu motions in the region 150–300 cm^{-1} , O and H atoms (and less pronounced also Cu) exhibit the largest amplitudes between 300 and 500 cm^{-1} . In the frequency range 350–500 cm^{-1} Cu-O scis-

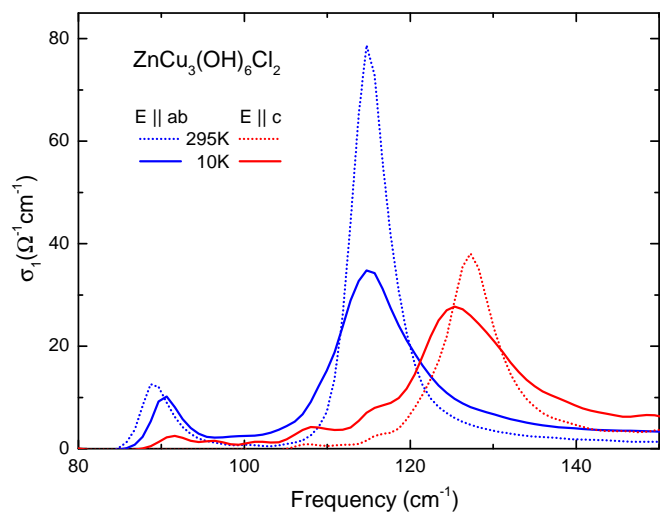


FIG. 4. Detailed view on the measured lowest-energy infrared vibrations of $\text{ZnCu}_3(\text{OH})_6\text{Cl}_2$. The magneto-elastic coupling is expected to be strongest for the modes at 115 cm^{-1} ($E \parallel ab$) and 125 cm^{-1} ($E \parallel c$), as expressed by the pronounced broadening and red-shift upon cooling.

soring and stretching are the dominant motions, with oxygen atoms experiencing the largest amplitude. For this reason, these and higher lying vibrations are most sensitive to Cu/Zn antisite disorder which is likely the origin of the splittings (400 and 700–820 cm^{-1} for $E \parallel c$; 900–1000 cm^{-1} for $E \parallel ab$) and the additional features with small intensity (600 cm^{-1} for $E \parallel c$). These splittings may also result from the lower monoclinic symmetry as suggested in Ref. 19. Above 3000 cm^{-1} the relative position of the out-of-plane hydrogen-related modes compared to those measured in-plane are in line with our calculations. We suggest that these O-H stretching vibrations around 3300–3500 cm^{-1} are also affected by antisite disorder, which explains their complex splitting: each proton is attached to an oxygen atom and feels the modified crystallographic surroundings in a similar way.

While qualitatively we can identify and characterize all infrared-active phonon modes, a quantitative comparison between measured and calculated phonon mode frequencies reveals some discrepancies that we attribute to different sources. For instance, the measured in-plane E_u^1 and E_u^2 modes at 90 and 115 cm^{-1} are observed at higher frequencies than the calculated doublet, 84.8 and 88.4 cm^{-1} , respectively. Actually, at low energies $h\nu \ll J \approx 180 - 190$ K, the magnetoelastic coupling is expected to manifest most strongly, so that this discrepancy may be largely attributed to the involvement of the spin degrees of freedom. The mismatch is generally more pronounced for vibrations that include deformations of the Cu-O-Cu bond lengths and angles within the kagome layer. For both polarizations the effect is largest for phonon modes close to 120 cm^{-1} which are also the modes exhibiting anomalous temperature dependence (see Fig. 4 and Ref. 21). In contrast, the measured

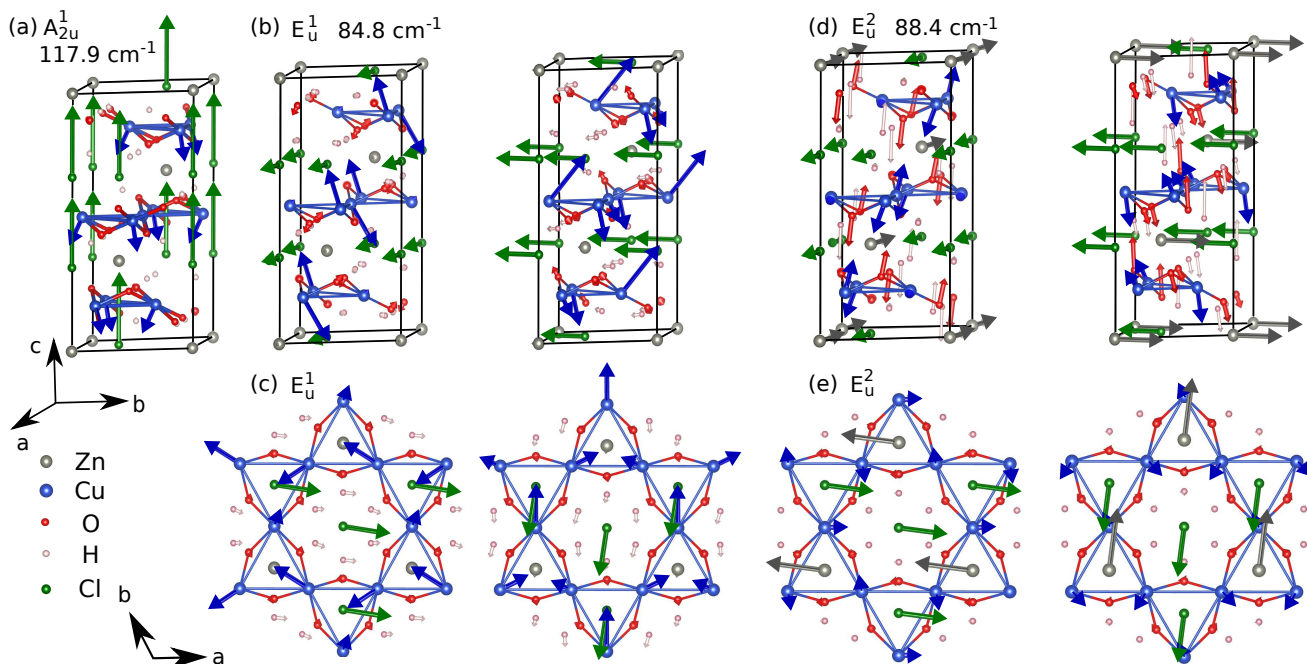


FIG. 5. The lowest-energy infrared vibrations according to our *ab initio* calculations. (a) A_{2u}^1 mode, (b, d) E_u^1 and E_u^2 phonon modes and (c, e) their projection onto the ab -plane, respectively.

modes around $700\text{--}1000\text{ cm}^{-1}$ appear at lower energies than computed. The range where the phonons oscillate at higher resonance frequencies than in the calculation ($0\text{--}700\text{ cm}^{-1}$) coincides with the two-magnon band seen by Raman spectroscopy²³. Interestingly, also the high-frequency proton modes above 3000 cm^{-1} – here considering the main peak – are subject to hardening by 5% despite $h\nu \gg J$. This is attributed to the description of hydrogen in the DFT calculations.

In the following we focus our main discussion on those features that exhibit anomalous temperature dependence, i.e. deviations from the common narrowing and blue-shift upon lowering the temperature.

In Fig. 4 we display the three measured lowest-energy infrared-active phonon modes of herbertsmithite and illustrate in Fig. 5 the corresponding atomic motions resulting from our calculations. The A_{2u} modes are dominated by Cl and Cu displacements along the c -direction [Fig. 5 (a)]. Panels (b-e) show the E_u^1 and E_u^2 modes and their $E \parallel ab$ projections corresponding to the measured 90 and 115 cm^{-1} peaks in Fig. 4, respectively.

We detect a clear relation between the amplitude of Cu atom displacements and the observed non-thermal broadening and red-shift which we associate with spin-phonon coupling. Distortions of the kagome lattice and, in particular, of the CuO_4Cl_2 octahedra due to atomic displacements directly influence the nearest-neighbor (super)exchange. Since for these phonon modes the frequency scales are comparable to the magnetic interaction scales, it is expected that the spins sense a modulation (distortion) of the other Cu sites which reflects in a transient change in J . If the phonon brings about a more

favourable spin configuration lowering the total energy, the system tends to stay "longer" in this arrangement which effectively reduces the spring constant k between the lattice sites and, thus, the resonance frequency. In this context, we would like to discuss recent reports of a monoclinic distortion^{19,20}. The lowest-energy in-plane modes in Fig. 5(b-e) indeed show Cl (and Zn) ions moving strictly within the ab -direction while, at the same time, the Cu atoms are displaced in an alternating fashion perpendicular to the kagome layers. The resulting deformations indeed break symmetry similar to the report in Ref. 19. The proposed stripe phase¹⁹ cannot be obtained by the in-plane projection of E_u^1 and E_u^2 but by their out-of-plane component, which is close to the movements in the right panels of Fig. 5 (b,d). Our analysis of the phonon spectrum and atomic displacements suggests that such measurements are compatible with E_u modes lowering the symmetry to m or 2 , and hint to a strong magnetoelastic coupling affecting and influencing the underlying spin system.

Further, at higher frequencies, although $h\nu \gg J$, the proton vibrations exhibit a pronounced non-thermal behavior, too. Despite being faster than the low-energy modes, the hydrogen atoms are bound to the oxygen sites, which keep moving on the slow time scales of the kagome-layer phonons. Thus, several proton oscillation cycles will be superimposed on the oxygen motions, such as the above mentioned CuO scissoring and stretching vibrations that are affected by the low-frequency spin-excitation continuum. This way, we expect that also the protons are affected by the effects of magneto-elastic coupling – at an energy $h\nu$ an order of magnitude larger than

J. This feature could possibly explain the higher resonance frequency observed in experiment as compared to the computed peak position.

In summary, we performed a comprehensive theoretical and experimental study of the lattice vibrations in $\text{ZnCu}_3(\text{OH})_6\text{Cl}_2$, providing insight into the mechanism of magneto-elastic coupling. Our *ab initio* calculations reproduce the vibrational peaks found in the infrared spectrum²¹. Quantitative differences between observed and computed resonance frequencies – the modes seen in experiment are blue-shifted compared to the calculation – coincide with the magnetic excitation background²³. The resulting atomic displacements and oscillation amplitudes reveal an intricate relation of kagome layer deformations with anomalous broadening and red shifts of the lowest-frequency phonons upon cooling. Surprisingly, even the O–H vibrations above 3000 cm^{-1} are susceptible to the low-energy magnetic degrees of freedom – an order of magnitude higher in frequency than $J \approx 180\text{ K}$. Moreover, the splitting of particular phonon modes in the ex-

perimental spectrum is attributed to the lower symmetry of the crystal resulting from disorder, providing a handle on antisite Cu/Zn exchange in $\text{ZnCu}_3(\text{OH})_6\text{Cl}_2$.

We expect that optical experiments as a function of pressure and magnetic field^{43,44}, as well as ultrasound studies⁴⁵ may provide additional information on the nature of magneto-elastic coupling and symmetry breaking in herbertsmithite. Further, having the full information about optical and acoustic phonons allows, in principle, to properly subtract these lattice contributions from the specific heat⁷ and isolate the spin entropy of the QSL.

ACKNOWLEDGMENTS

We thank M. R. Norman for fruitful discussions. The project was supported by the Deutsche Forschungsgemeinschaft (DFG) through grant VA117/15-1.

*Y.L. and A.P. contributed equally to this work.

-
- ¹ M. R. Norman, *Rev. Mod. Phys.* **88**, 041002 (2016).
² V. R. Shaginyan, A. Z. Msezane, M. Y. Amusia, J. W. Clark, G. S. Japaridze, V. A. Stephanovich, and Y. S. Leevik, *Condensed Matter* **4** (2019).
³ H. O. Jeschke, F. Salvat-Pujol, and R. Valentí, *Phys. Rev. B* **88**, 075106 (2013).
⁴ P. Mendels, F. Bert, M. A. de Vries, A. Olariu, A. Harrison, F. Duc, J. C. Trombe, J. S. Lord, A. Amato, and C. Baines, *Phys. Rev. Lett.* **98**, 077204 (2007).
⁵ T.-H. Han, J. S. Helton, S. Chu, D. G. Nocera, J. A. Rodriguez-Rivera, C. Broholm, and Y. S. Lee, *Nature* **492**, 406 (2012).
⁶ M. P. Shores, E. A. Nytko, B. M. Bartlett, and D. G. Nocera, *J. Am. Chem. Soc.* **127**, 13462 (2005).
⁷ J. S. Helton, K. Matan, M. P. Shores, E. A. Nytko, B. M. Bartlett, Y. Yoshida, Y. Takano, A. Suslov, Y. Qiu, J.-H. Chung, D. G. Nocera, and Y. S. Lee, *Phys. Rev. Lett.* **98**, 107204 (2007).
⁸ M. A. de Vries, J. R. Stewart, P. P. Deen, J. O. Piatek, G. J. Nilsen, H. M. Rønnow, and A. Harrison, *Phys. Rev. Lett.* **103**, 237201 (2009).
⁹ T. Imai, E. A. Nytko, B. M. Bartlett, M. P. Shores, and D. G. Nocera, *Phys. Rev. Lett.* **100**, 77203 (2008).
¹⁰ A. Olariu, P. Mendels, F. Bert, F. Duc, J. C. Trombe, M. A. de Vries, and A. Harrison, *Phys. Rev. Lett.* **100**, 87202 (2008).
¹¹ R. R. P. Singh and D. A. Huse, *Phys. Rev. B* **76**, 180407 (2007).
¹² Y. Ran, M. Hermele, P. A. Lee, and X.-G. Wen, *Phys. Rev. Lett.* **98**, 117205 (2007).
¹³ S. Dejenbrock, I. P. McCulloch, and U. Schollwöck, *Phys. Rev. Lett.* **109**, 067201 (2012).
¹⁴ Y. Iqbal, F. Becca, S. Sorella, and D. Poilblanc, *Phys. Rev. B* **87**, 060405 (2013).
¹⁵ M. Fu, T. Imai, T.-H. Han, and Y. S. Lee, *Science* **350**, 655 LP (2015).
¹⁶ Y.-C. He, M. P. Zaletel, M. Oshikawa, and F. Pollmann, *Phys. Rev. X* **7**, 031020 (2017).
¹⁷ H. J. Liao, Z. Y. Xie, J. Chen, Z. Y. Liu, H. D. Xie, R. Z. Huang, B. Normand, and T. Xiang, *Phys. Rev. Lett.* **118**, 137202 (2017).
¹⁸ P. Khuntia, M. Velazquez, Q. Barthlemy, F. Bert, E. Kermarrec, A. Legros, B. Bernu, L. Messio, A. Zorko, and P. Mendels, *arXiv:1911.09552* (2019).
¹⁹ N. J. Laurita, A. Ron, J. W. Han, A. Scheie, J. P. Shekellon, R. W. Smaha, W. He, J.-J. Wen, J. S. Lee, Y. S. Lee, M. R. Norman, and D. Hsieh, *arXiv:1910.13606* (2019).
²⁰ A. Zorko, M. Herak, M. Gomilšek, J. van Tol, M. Velázquez, P. Khuntia, F. Bert, and P. Mendels, *Phys. Rev. Lett.* **118**, 17202 (2017).
²¹ A. B. Sushkov, G. S. Jenkins, T.-H. Han, Y. S. Lee, and D. H. D. J. *Phys. Condens. Matter* **29**, 95802 (2017).
²² A. Pustogow, Y. Li, I. Voloshenko, P. Puphal, C. Krellner, I. I. Mazin, M. Dressel, and R. Valentí, *Phys. Rev. B* **96**, 241114(R) (2017).
²³ D. Wulferding, P. Lemmens, P. Scheib, J. Röder, P. Mendels, S. Chu, T. Han, and Y. S. Lee, *Phys. Rev. B* **82**, 144412 (2010).
²⁴ A. B. Sushkov, O. Tchernyshyov, W. R. II, S. W. Cheong, and H. D. Drew, *Phys. Rev. Lett.* **94**, 137202 (2005).
²⁵ L. J. Sandilands, Y. Tian, K. W. Plumb, Y.-J. Kim, and K. S. Burch, *Phys. Rev. Lett.* **114**, 147201 (2015).
²⁶ T. H. Han, J. S. Helton, S. Chu, A. Prodi, D. K. Singh, C. Mazzoli, P. Müller, D. G. Nocera, and Y. S. Lee, *Phys. Rev. B* **83**, 100402 (2011).
²⁷ R. S. W. Braithwaite, K. Mereiter, W. H. Paar, and A. M. Clark, *Mineral. Mag.* **68** (2004).
²⁸ A. Togo, F. Oba, and I. Tanaka, *Phys. Rev. B* **78**, 134106 (2008).
²⁹ A. Togo and I. Tanaka, *Scripta Materialia* **108**, 1 (2015).
³⁰ K. Parlinski, Z. Q. Li, and Y. Kawazoe, *Phys. Rev. Lett.* **78**, 4063 (1997).
³¹ J. P. Perdew, K. Burke, and M. Ernzerhof, *Phys. Rev. Lett.* **77**, 3865 (1996).
³² P. E. Blöchl, *Phys. Rev. B* **50**, 17953 (1994).
³³ G. Kresse and J. Hafner, *Phys. Rev. B* **47**, 558 (1993).

- ³⁴ G. Kresse and J. Furthmüller, *Phys. Rev. B* **54**, 11169 (1996).
- ³⁵ G. Kresse and J. Furthmüller, *Computational Materials Science* **6**, 15 (1996).
- ³⁶ A. Pustogow, M. Bories, A. Löhle, R. Rösslhuber, E. Zhukova, B. Gorshunov, S. Tomić, J. A. Schlueter, R. Hübner, T. Hiramatsu, Y. Yoshida, G. Saito, R. Kato, T.-H. Lee, V. Dobrosavljević, S. Fratini, and M. Dressel, *Nat. Mater.* **17**, 773 (2018).
- ³⁷ M. Dressel and A. Pustogow, *J. Phys. Condens. Matter* **30**, 203001 (2018).
- ³⁸ J. Ferber, K. Foyevtsova, H. O. Jeschke, and R. Valentí, *Phys. Rev. B* **89**, 205106 (2014).
- ³⁹ M. Dressel, P. Lazić, A. Pustogow, E. Zhukova, B. Gorshunov, J. A. Schlueter, O. Milat, B. Gumhalter, and S. Tomić, *Phys. Rev. B* **93**, 81201 (2016).
- ⁴⁰ M. Matsuura, T. Sasaki, S. Iguchi, E. Gati, J. Müller, O. Stockert, A. Piovano, M. Böhm, J. T. Park, S. Biswas, S. M. Winter, R. Valentí, A. Nakao, and M. Lang, *Phys. Rev. Lett.* **123**, 027601 (2019).
- ⁴¹ D. V. Pilon, C. H. Lui, T. H. Han, D. Shrekenhamer, A. J. Frenzel, W. J. Padilla, Y. S. Lee, and N. Gedik, *Phys. Rev. Lett.* **111**, 127401 (2013).
- ⁴² See Supplemental Material which contains all 54 phonon modes for Herbertsmithite.
- ⁴³ D. P. Kozlenko, A. F. Kusmartseva, E. V. Lukin, D. A. Keen, W. G. Marshall, M. A. de Vries, and K. V. Kamenev, *Phys. Rev. Lett.* **108**, 187207 (2012).
- ⁴⁴ T. Biesner and E. Uykur, “Pressure-Tuned Interactions in Frustrated Magnets: Pathway to Quantum Spin Liquids?” (2020).
- ⁴⁵ J. Wosnitzer, S. A. Zvyagin, and S. Zherlitsyn, *Reports on Progress in Physics* **79**, 074504 (2016).